SICE Annual Conference 2008
August 20-22, 2008, The University Electro-Communications, Japan

The Control Algorithm Enabling Natural Physical Interaction with Humanoid Robot Arm Having Joint Flexibility

Dzmitry Tsetserukou, Naoki Kawakami, and Susumu Tachi

Department of Information Physics and Computing, University of Tokyo, Tokyo, Japan
(Tel : +81-3-5841-6917; E-mail: dima_teterukov@ipc.i.u-tokyo.ac.jp)

Abstract: The paper is concentrated on control of humanoid robot arm intended for operation in unstructured human being-environment. A variable impedance control strategy was elaborated to increase the robot functionality and to achieve human-like dynamics of interaction. The detailed design procedure of the lead controller enabling improvement of transient response is presented. The experimental results show that proposed approach not only provides safe interaction of robot arm with a person, but also improves the effectiveness of contact task performance.

Keywords: Variable impedance control, safe human-robot interaction, joint flexibility, teleoperation.

1. INTRODUCTION

In designing the human-friendly robots intended for physical cooperation, the primary concern is safety issues. Unexpected collisions should be managed in such a way that contact forces do not pose a danger for human beings. Generally, two techniques of safe interaction with robot are well recognized, namely, passive compliance control and active force control.

Passive compliance of robot can be achieved by integration of mechanical leaf springs [1] or variable stiffness actuators [2] into each joint gaining fast response to external disturbance. However, they also can cause vibrations with high amplitude that destabilize the dynamic behavior. Additionally, the robot control in such cases is complicated by many unknown parameters (e.g. actuator stiffness and damping). Pneumatic muscles with low weight and inherent compliant behavior due to air compressibility are also exploited in human-friendly robots [3]. The limitations of such actuators are nonlinear flexible characteristics, long reaction time, and small position accuracy.

Active force control implies that the robot structure is stiff enough to provide high position accuracy; and contact ability with environment is achieved by excessive sensory system feedback [4]. However, due to the time lag induced by sampling process, such robots pose dangerousness at the moment of impact.

In our robot design we embodied advantages of both methods. The developed anthropomorphic manipulator having 4-DOF arm and 8-DOF hand (Fig. 1(c)) is capable of safe interaction with environment. To realize the safe physical contact of entire robot arm structure with human, the developed optical torque sensors were distributed into each joint of the robot arm. When contact with environment occurs, manipulator automatically generates compliant motion according to the measured external torque values (active control). On the other hand, the torque sensors designed with low stiffness mitigate the impact forces on the initial state of contact transient (passive control).

The teleoperation system aimed at performing the cooperative tasks with humans is presented in Fig. 1.

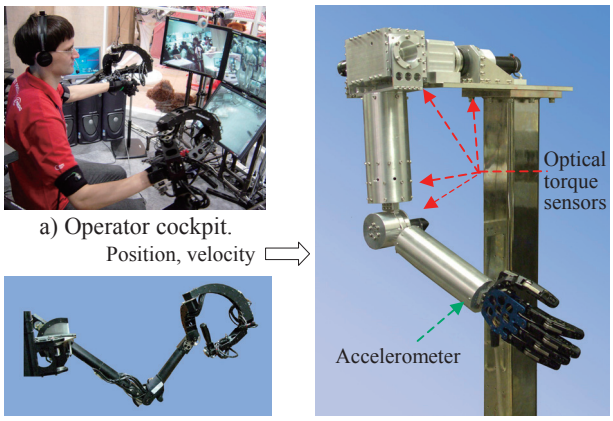

a) Operator cockpit. b) Master arm. c) Developed robot arm.

Fig. 1.Robot teleoperation system.

The robot arm is controlled by operator's motion (Fig. 1(a)). During operation of manipulator the movement information (position, orientation, and velocity) is acquired through encoders of the motors installed into each joint of the master arm (Fig. 1(b)). The motion of the human elbow is controlled by the tilt sensor.

There are several conflicting requirements on the choice of dynamics parameters of impedance model to provide effectiveness and functionality of robot in tasks of physical interactions. For example, while accomplishing service tasks for human in the autonomous mode, it is required to provide high stiffness (to ensure small position error during object handling) and high damping (for good velocity tracking). In the case of collision, the low stiffness is necessary to reduce the impact forces. We elaborated a new methodology for joint impedance parameter regulation based on human-like ability to softly interact with environment.

The paper also focuses on the vibration damping control to attenuate oscillations in heavily loaded joints during acceleration and deceleration stages. The algorithm providing smooth continuous motion while interacting with environment is detailed. Experimental results of variable impedance control and vibration damping control are discussed.

PR0001/08/0000-2777 ¥400 © 2008 SICE

2. JOINT IMPEDANCE CONTROL

2.1 Impedance control

To achieve skillful human-like behavior, the robot has to be able to change its dynamic characteristics depending on time-varying interaction forces. The most efficient method of controlling the interaction between a manipulator and an environment is impedance control. This approach enables to regulate response properties of robot to external forces through modifying the mechanical impedance parameters (Fig. 2).

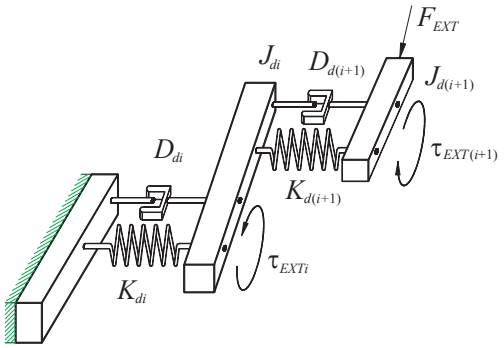

Fig. 2 Presentation of the local impedance control.

The desired impedance properties of *i-th* joint of manipulator can be expressed as:

$$J_{di}\Delta\ddot{\theta}_i + D_{di}\Delta\dot{\theta}_i + K_{di}\Delta\theta_i = \tau_{EXTi};\ \Delta\theta_i = \theta_{ci} - \theta_{di}, \qquad (1)$$

where J_{di}, D_{di}, K_{di} are the desired inertia, damping, and stiffness of *i-th* joint, respectively; τ_{EXTi} is torque applied to *i-th* joint, $\Delta\theta_i$ is the difference between the current compliant angle θ_{ci} and desired one θ_{di}.

The state-space presentation of the Eq. (1) is:

$$\begin{bmatrix}\Delta\dot{\theta}_i \\ \dot{\upsilon}_i\end{bmatrix} = \begin{bmatrix}0 & 1 \\ -K_d/J_d & -D_d/J_d\end{bmatrix}\begin{bmatrix}\theta_i \\ \upsilon_i\end{bmatrix} + \begin{bmatrix}0 \\ 1/J_d\end{bmatrix}\tau_{EXTi}(t), \qquad (2)$$

where υ_i is the state variable ($\upsilon_i = \Delta\dot{\theta}_i$).

The discrete presentation of Eq. (2) with sampling time of T is needed for program code implementation:

$$\begin{bmatrix}\Delta\theta_{k+1} \\ \Delta\dot{\theta}_{k+1}\end{bmatrix} = A_d\begin{bmatrix}\Delta\theta_k \\ \Delta\dot{\theta}_k\end{bmatrix} + B_d T_{EXT(k)}\ . \qquad (3)$$

For the fastest non-oscillatory response on the external force (when the eigenvalues of matrix A λ_1 and λ_2 are real and equal), we have:

$$A_d = e^{\lambda_1 T}\begin{bmatrix}1-\lambda_1 T & T \\ -K_d T/J_d & 1-\lambda_1 T - D_d T/J_d\end{bmatrix}, \qquad (4)$$

$$B_d = \left(A_d - I\right)A^{-1}B = \frac{1}{K_d}\begin{bmatrix}1-e^{\lambda_1 T}(1-\lambda_1 T) \\ \left(D_d/(2J_d)\right)^2 T e^{\lambda_1 T}\end{bmatrix}, \qquad (5)$$

where I is the identity matrix.

2.2 Variable joint impedance control

The limitation of impedance control with constant coefficients is that it cannot provide adaptation of robot dynamic behavior to different tasks. To overcome this, two approaches were developed: adaptive [5] and functional [6] adjustments of impedance parameters. We have proposed a new method based on human-like ability to softly interact with environment.

It was found that humans adjust their joint stiffness to accommodate changes in surface stiffness [7]. Furthermore, the research on impedance characteristics of human arm shows that, while pushing the object naturally, human arm stiffness and damping behavior can be approximated by exponential curves [8].

To impart the human-like damping and stiffness behavior to robot arm interacting with environment, we introduce the exponential functional dependency between sensed force and stiffness. For service task accomplishment (when high stiffness and damping of joints is required), the thresholds of external disturbance torque τ_{EXTth} was assigned for each joint of robot arm.

The desired stiffness K_{d1} for the case of service task is calculated based on the maximum deflection of joint angle $\Delta\theta_{max}$ caused by external torque τ_{EXT}:

$$K_{d1} = \frac{\tau_{EXT}}{\Delta\theta_{max}}\ . \qquad (6)$$

It was defined that external torque of 1 Nm results in $\Delta\theta_{max}$ of 0.1 rad yielding K_{d1} of 10 Nm/rad. The desired damping D_{d1} is expressed as:

$$D_{d1} = 2\zeta\sqrt{K_{d1}J_{d1}}\ . \qquad (7)$$

Damping coefficient ζ of 1.05 and desired inertia J_{d1} of 0.1 kg·m^2 was defined to achieve fast non-oscillatory response giving D_{d1} of 2.1 Nm·s/rad. These parameters are valid till the interaction force does not cause the overload of robot arm. When sensed torque value exceeds the threshold, robot recognizes this condition as collision or human following motion mode, and adjusts its dynamics parameters to provide smooth natural interaction. To realize such continuous change of dynamics, we are using exponential relation between external disturbance torque and desired stiffness:

$$K_{d2} = K_{d1}e^{\mu(\tau_{EXT} - \tau_{EXTth})}, \qquad (8)$$

where K_{d2} is the variable desired stiffness aimed at soft interaction; μ is the joint stiffness reduction coefficient.

The desired damping is adjusted to prevent force responses from being too sluggish while changing stiffness values, and to ensure contact stability:

$$D_{d2} = 2\zeta\sqrt{K_{d2}J_{d1}} = 2\zeta e^{0.5\mu(\tau_{EXT} - \tau_{EXTth})}\sqrt{K_{d1}J_{d1}}\ . \qquad (9)$$

Then, Eq. (1) for variable joint impedance controller is written as:

$$\tau_{EXTi} = J_{di}\Delta\ddot{\theta}_i + 2\zeta e^{0.5\mu(\tau_{EXTi}-\tau_{EXThi})}\sqrt{K_{di1}J_{di1}}\Delta\dot{\theta}_i + \\ + K_{di1}e^{\mu(\tau_{EXTi}-\tau_{EXThi})}\Delta\theta_i;\ \Delta\theta_i = \theta_{ci} - \theta_{di}\ . \qquad (10)$$

To ensure the effectiveness of service task accomplishment, we decided to implement admittance control. In this algorithm, compliant trajectory generated by the impedance controller is tracked by the PD control loop. During the experiment, the interaction with robot arm was performed to exceed join torque threshold level of 0.6 Nm. The experimental results for the elbow joint – applied torque, stiffness and damping, impedance trajectory with constant and variable coefficients – are shown in Figs. 3(a)~3(d), respectively.

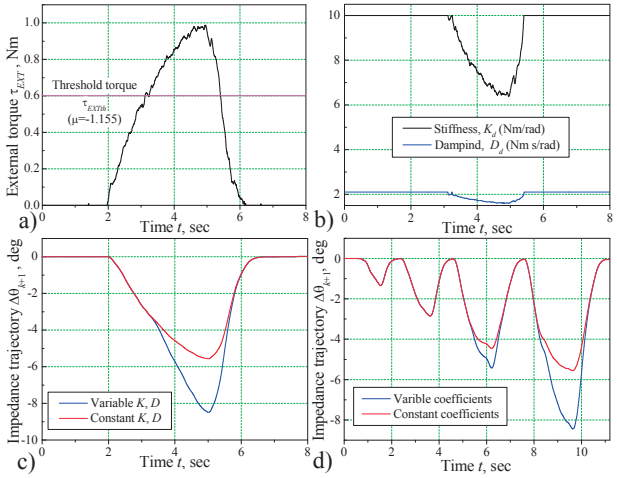

Fig. 3 Experimental results.

The plots represented in Figs. 3(c), 3(d) show that the proposed variable impedance control provides smoother trajectory while avoiding impact than the impedance control with constant coefficients.

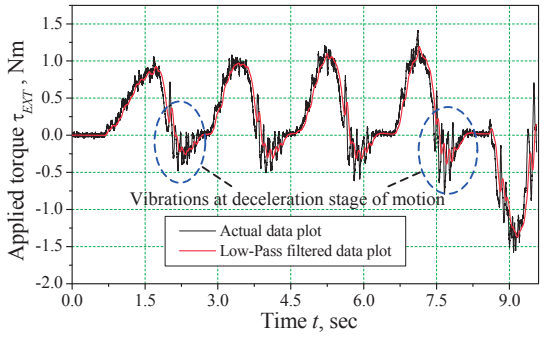

Fig. 4 Vibrations in heavily loaded joint.

However, experimental results of human-robot interaction for the inertially loaded first joint show that despite the smooth trajectory generated by the admittance controller, the vibratory behavior is recorded by torque sensor (Fig. 4).

3. THE MODEL OF ROBOT WITH JOINT FLEXIBILITY

3.1 Dynamic model of flexible robot joint

Flexibility introduced into robot arm joint through harmonic drive and torque sensors changes the dynamic behavior of mechanical structure. Robot joint with compliance can be represented as two-inertia system (Fig. 5).

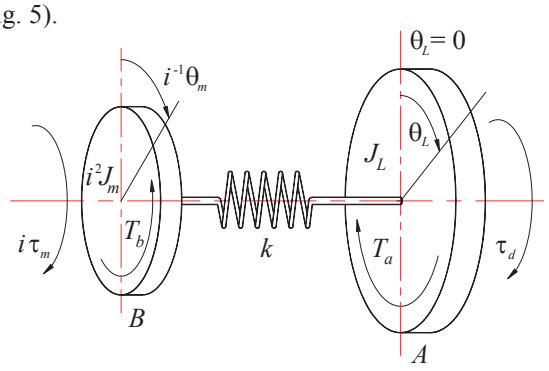

Fig. 5 Two-inertia vibration model of robot joint.

The dynamic equations of the n-DOF manipulator with joint compliance in joint space coordinates can be obtained by D'Alembert's principle. The equations of static equilibrium for mass A (Eq. (11)) and mass B (Eq. (12)) ignoring damping are as follows:

$$\begin{cases} J_L(\theta_L)\ddot{\theta}_L = k\left(i^{-1}\theta_m - \theta_L\right) + \tau_d & (11) \\ J_m\ddot{\theta}_m = -i^{-1}k\left(i^{-1}\theta_m - \theta_L\right) + \tau_m & (12) \\ \tau_d = \tau_{EXT} - G(\theta_L) - C(\theta_L,\dot{\theta}_L)\dot{\theta}_L & (13) \\ \tau = k\left(i^{-1}\theta_m - \theta_L\right), & (14) \end{cases}$$

where $\theta_L, \dot{\theta}_L, \ddot{\theta}_L \in R^n$ are the vectors of the link angles, the link angular velocities, and the link angle accelerations, respectively; $\theta_m, \ddot{\theta}_m \in R^n$ are the vectors of motor angles, and the motor angle accelerations, respectively; $k \in R^{n\times n}$ is the diagonal matrix of joint stiffness; $i \in R^n$ is the vector of gear reduction ratios; $J_L(\theta_L) \in R^{n\times n}$ is the symmetric, positive definite link inertia matrix; $J_m \in R^{n\times n}$ is the diagonal, positive definite rotor inertia matrix; $\tau_d \in R^n$ is the vector of disturbance torques; $\tau_m \in R^n$ is the vector of torques applied by motor; $\tau_{EXT} \in R^n$ is the vector of applied external joint torques; $G(\theta_L) \in R^n$ is the vector of gravitational torques; $C(\theta_L,\dot{\theta}_L) \in R^n$ represents the vector of Coriolis and centrifugal torques; $\tau_m \in R^n$ is the vector of torques applied by motor; the torque in the shaft $\tau \in R^n$ is directly proportional to twist angle $\theta = (i^{-1}\theta_m - \theta_L)$.

The natural frequency of two-mass system ω_n and natural frequency of one-mass robot joint ω_L are derived from the following equations:

$$\omega_n = \sqrt{k\left(\frac{1}{i^2 J_m} + \frac{1}{J_L}\right)}, \qquad \omega_L = \sqrt{\frac{k}{J_L}}\ . \qquad (15)$$

The damped response of motor dynamics can be achieved by D-gain augmentation of position controller. The technique of vibration attenuation by using negative

torque feedback was reported [9,4]. The idea behind this approach is that negative torque feedback reduces the effective inertia of the motor rotor. However, whereas it can suppress the vibrations to some extent, it cannot affect the main source of vibrations, namely, the inertial loading. To design the vibration damping controller the oscillation parameter determination is needed.

3.2 Oscillation parameter identification

The approach proposed by us is to employ position feedback based on information from accelerometer and lead controller to improve the damping property of the compliant robot joint. To illustrate the torsional vibrations caused by unbalanced inertial load, let us consider dynamic model of robot arm given in Fig. 6.

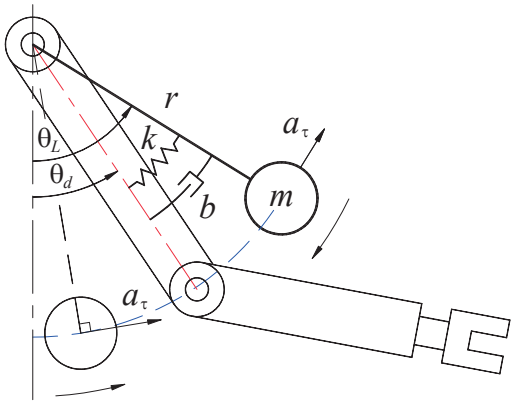

Fig. 6 Graphical presentation of torsional vibrations.

The desired trajectory generated by master arm movement or, in case of interaction with environment by impedance controller, is described by angle θ_d. The flexibility of the joint produces vibrations about *Z*-axis of corresponding joint. We can neglect the influence of gravitational force due to small vibration angle change. Using the balance equations of forces acting on the joint we can write:

$$J_L\ddot{\theta}_L + b\dot{\theta}_L + k\left(\theta_L - \theta_d\right) = 0\,, \tag{16}$$

where $\theta_L, \dot{\theta}_L, \ddot{\theta}_L$ are actual angle, angular speed and angular acceleration of the link, respectively; *b* is a viscous damping constant.

By Laplace transform we get the following transfer function:

$$\frac{\theta_L(s)}{\theta_d(s)} = \frac{k}{J_L s^2 + bs + k} = \frac{\omega_L^2}{s^2 + 2\zeta\omega_L s + \omega_L^2}\,, \tag{17}$$

where ζ is the damping coefficient.

The oscillation periods of the angle of link, angular acceleration, and angular speed are identical. Therefore, from analysis of the angular acceleration signal we can obtain the values of natural frequency and damping coefficient. The three-axis accelerometer with sensitivity of 600 mV/G was used. The accelerometer layout along with associated coordinate systems are given in Fig. 7.

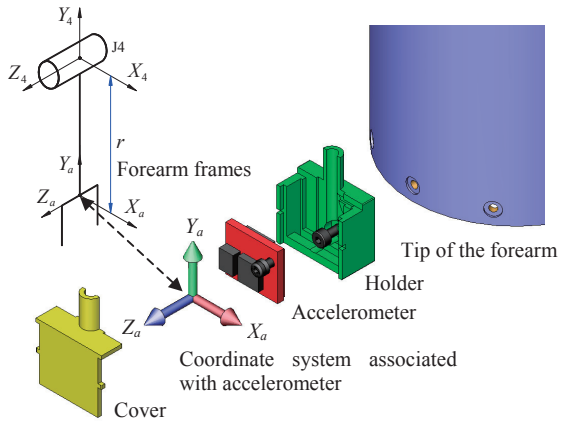

Fig. 7 Accelerometer layout.

As seen from Fig. 7, the linear tangential acceleration a_τ corresponds to the *X* component of accelerometer output. Angular acceleration of robot link equals a_τ/r.

While dynamic testing, elbow joint was fixedly mounted and the system was exited by impulse force. The data acquisition system recorded the subsequent vibrations with a sampling rate of 100 kHz (Fig. 8). To eliminate high frequency noise, the digital low-pass filter was deployed with cut-off frequency of 100 Hz.

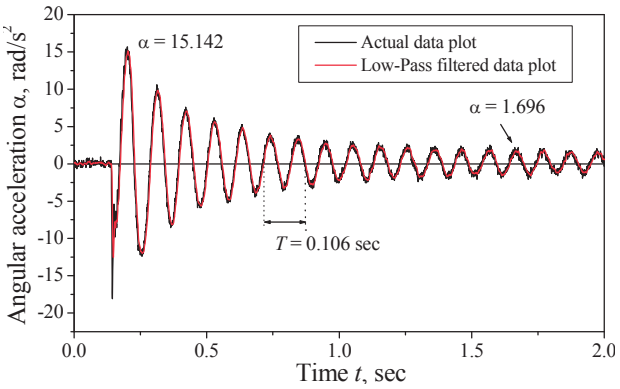

Fig. 8 Impulse response of the robot link.

The calculated damping coefficient ζ of 0.0249 and natural frequency of robot link ω_L of 58.3 rad/sec indicate that system is lightly damped and oscillation-damping controller is, therefore, needed.

4. DESIGN OF VIBRATION DAMPING CONTROLLER

We are proposing to use load angle position feedback and lead compensator to damp the undesirable vibrations. The angular position can be calculated from accelerometer data by means of double integration. The high-pass filtering with cut-off angular frequency ω_{HP} of 3 rad/sec is necessary to eliminate the drift of the signal. The transfer function of double integrator with high-pass filter is expressed as:

$$\frac{y(s)}{u(s)}=\frac{\theta_L(s)}{\ddot{\theta}_L(s)}=\frac{1}{s^2}\frac{s^2}{\left(s+\omega_{HP}\right)^2}=\frac{1}{\left(s+\omega_{HP}\right)^2}. \quad (18)$$

To improve the system performance and to meet the performance specification, we should design the compensator. Such properties of lead compensator as speeding the response up and increasing the stability of the system make it the preferable one. The transfer function of lead compensator is written as:

$$G_c(s)=\frac{y(s)}{u_c(s)}=\frac{K}{\alpha}\frac{\left(s+\omega_z\right)}{\left(s+\omega_p\right)}=\frac{K}{\alpha}\frac{\left(s+\omega_z\right)}{\left(s+\omega_z/\alpha\right)}, \quad (19)$$

where ω_z, ω_p are the zero and pole; K is the constant gain [10].

The block diagram of the closed loop system with lead compensator is shown in Fig. 9.

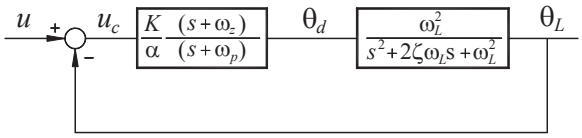

Fig. 9 System with lead compensator.

First, we determine the gain K to satisfy the steady-state error e_{ss} (less then 1.0% for a unit step function):

$$e_{ss}=\frac{1}{1+G_c(0)G(0)}\le 0.01. \quad (20)$$

The calculated value of K is 99. The specification of system damping coefficient of 0.55 provides the value of required phase margin ψ defined by:

$$\psi=\tan^{-1}\frac{2\zeta}{\sqrt{-2\zeta^2+\sqrt{1+4\zeta^2}}}. \quad (21)$$

The phase margin ψ derived from Eq. (21) is 55.7°. Value of the uncompensated system phase margin is as low as 0.29°. Therefore, we need to add phase lead, which satisfies required damping property of the system. With account of compensation of shift in the gain crossover frequency the maximum required phase lead angle ψ_{max} is approximately 60°. The coefficient α is computed from:

$$\alpha=\frac{1-\sin(\psi_{\max})}{1+\sin(\psi_{\max})}. \quad (22)$$

The new gain crossover frequency ω_c for total compensated system is given by intersection of line $20\log_{10}\sqrt{\alpha}$ and bode magnitude plot (for α of 0.0718, ω_c=-11.44 dB). The final step is to calculate corner frequencies ω_z, ω_p. Taking advantage of the fact that the maximum phase lead angle ψ_{max} occurs at the geometric mean of two corner frequencies ω_z, ω_p, we can get:

$$\omega_z=\omega_c\sqrt{\alpha}, \qquad \omega_p=\omega_c/\sqrt{\alpha}. \quad (23)$$

The values of ω_z and ω_p equal 321 rad/sec and 4477 rad/sec.

The magnitude curve and phase-angle curve for the compensated system are shown in Fig. 10. The phase and gain margins are 60 deg and +∞, respectively. Therefore, compensated system meets both the steady-state and the relative stability requirements.

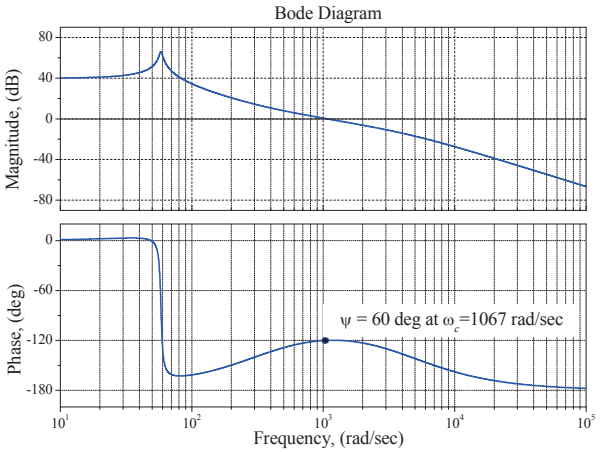

Fig. 10 Bode diagram.

Thus, the desirable transient behavior was achieved through usage of lead compensator.

From Eq. (19) the state-space representation of the lead controller is obtained:

$$\begin{cases}\dot{x}(t)=-\omega_p x(t)+u_c(t) & (24)\\ y(t)=\frac{K}{\alpha}\left((\omega_z-\omega_p)x(t)+u_c(t)\right). & (25)\end{cases}$$

where $x(t)$ is the state vector, $y(t)$ is the output, $u_c(t)$ is the input.

Solution of the differential equation for $x(t)$ is:

$$x(t)=e^{-\omega_p t}x(0)+\int_0^t e^{-\omega_p(t-\tau)}u_c(\tau)d\tau. \quad (26)$$

For calculation step k and sampling time T we have:

$$x_{k+1}=e^{-\omega_p T}x_k+\left((1-e^{-\omega_p T})/\omega_p\right)U_{c(k)} \quad (27)$$

$$y_k=\theta_{d(k)}=\frac{K}{\alpha}\left((\omega_z-\omega_p)x_k+U_{c(k)}\right), \quad (28)$$

where $U_{c(k)}$ is the discrete input signal.

The obtained value of desired load angle $\theta_{d(k)}$ is then processed by PD control loop (Fig. 11). To evaluate the performance of the proposed damping controller, the dynamic testing was conducted.

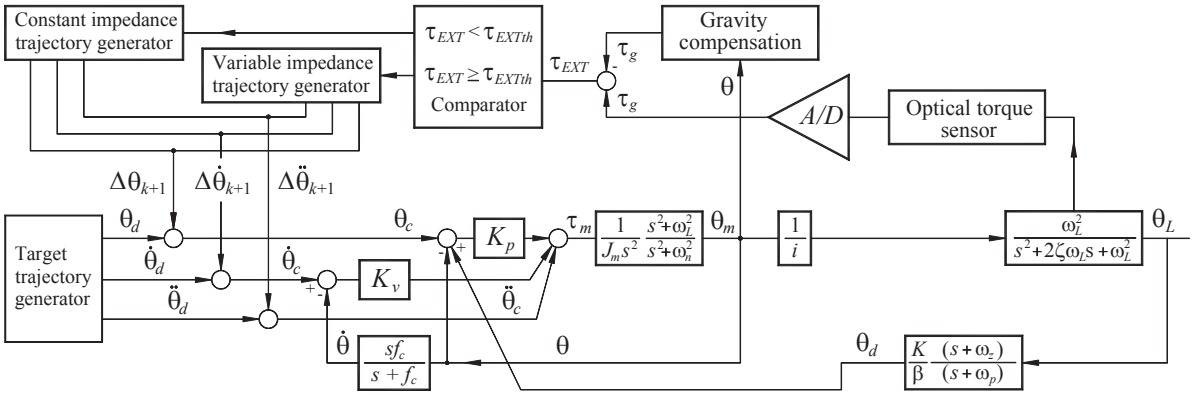

Fig. 11 Block diagram of designed controller.

Experimental results show the successful damping of oscillation magnitude (Fig. 12). The system resists the quick change in angular speed, and, therefore, provides more smooth dynamic behavior.

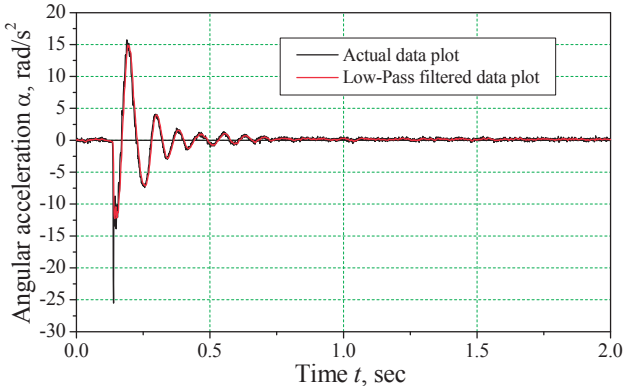

Fig. 12 Impulse response of system with controller.

It is important to emphasize here, that theoretically calculated control gain and feedback gain must be adjusted while experiment conducting. Too high gains can cause increasing sensitivity to noise signal.

5. CONCLUSIONS

A variable impedance control strategy was elaborated to increase the robot functionality and to achieve human-like dynamics of interaction. The effectiveness of the position-based variable impedance control for providing safe human-robot interaction was experimentally illustrated on a whole-sensitive robot arm. Tactile sensation of soft friendly interaction with robot arm was achieved.

The flexibility of robot joint caused by compliant elements, such as torque sensors and harmonic drives, produces significant effect on dynamics of robot. To compensate flexibility effect, first, we elaborated the dynamic model of the robot joint as two-inertia system. The oscillation parameters were determined by using experimental data and analytical equations. The system with lead compensator and angular position of the load feedback is proposed to damp undesired vibrations. The experimental results show high performance of the developed controller in terms of successful damping of vibrations.

Acknowledgments. The research is supported in part by a Japan Society for the Promotion of Science (JSPS) Postdoctoral Fellowship for Foreign Scholars.

REFERENCES

[1] H. Iwata, S. Kobashi, T. Aono, S. Sugano, "Design of Anthropomorphic 4-DOF Tactile Interaction Manipulator with Passive Joints", *IEEE/RSJ Int. Conf. Intelligent Robots and Systems*, Edmonton, pp. 1785-1790, 2005.

[2] A. Bicchi and G. Tonietti, "Fast and Soft Arm Tactics: Dealing with the Safety-performance Trade-off in Robot Arms Sesign and Control", *IEEE Robotics and Automation Magazine*, Vol.11, No.2, pp. 22-33, 2004.

[3] D. G. Cadwell, A. Medrano-Cerda, M. Goodwin, "Control of Pneumatic Muscle Actuators", *IEEE Control Systems Journal*, Vol. 15, No. 1, pp. 40-48, 1995.

[4] A. Albu-Schaffer and G. Hirzinger, "State Feedback Controller for Flexible Joint Robots: a Globally Stable Approach Implemented on DLR`s Light Weight Robots", *IEEE/RSJ Int. Conf. Intelligent Robots and Systems*, Takamatsu, pp. 1087-1093, 2000.

[5] R. Carelli and R. Kelly, "Adaptive Impedance/force Controller for Robot Manipulators", *IEEE Transactions on Automatic Control*, Vol. 36, pp. 967-972, 1991.

[6] T. Tsumugiwa, R. Yokogawa, K. Hara, "Variable Impedance Control based on Estimation of Human Arm Stiffness for Human-robot Cooperative Calligraphic Task", *IEEE Int. Conf. Robotics and Automation*, Washington, DC, pp. 644-650, 2002.

[7] D. P. Ferris and C. T. Farley, "Interaction of Leg Stiffness and Surface Stiffness During Human Hoping", *Journal of Applied Physiology*, Vol. 82, No. 1, pp. 15-22, 1997.

[8] M. M. Rahman, R. Ikeura, K. Muzutani, "Investigating the Impedance Characteristics of Human Arm for Development of Robot to Cooperate with Human Operators", *IEEE Int. Conf. Systems, Man and Cybernetics*, Tokyo, pp. 676-681, 1999.

[9] G. Zhang and J. Furusho, "Control of Robot Arms Using Joint Torque Sensors", *IEEE Int. Conf. Robotics and Automation*, Albuquerque, pp. 3148-3153, 1997.

[10] K. Ogata, *Modern Control Engineering*, Upper Saddle River, NJ: Prentice-Hall, 1997.